The Astrophysical Journal, 671: L000–L000, 2007 December 20

MERGED IONIZATION/DISSOCIATION FRONTS IN PLANETARY NEBULAE[1]

William J. Henney,[2] R. J. R. Williams,[3] Gary J. Ferland,[4] Gargi Shaw,[4] and C. R. O'Dell[5]

Received 2007 October 16; accepted 2007 October 31; published 2007 November 21

ABSTRACT

The hydrogen ionization and dissociation front around an ultraviolet radiation source should merge when the ratio of ionizing photon flux to gas density is sufficiently low and the spectrum is sufficiently hard. This regime is particularly relevant to the molecular knots that are commonly found in evolved planetary nebulae, such as the Helix Nebula, where traditional models of photodissociation regions have proved unable to explain the high observed luminosity in H_2 lines. In this paper we present results for the structure and steady state dynamics of such advection-dominated merged fronts, calculated using the Cloudy plasma/molecular physics code. We find that the principal destruction processes for H_2 are photoionization by extreme ultraviolet radiation and charge-exchange reactions with protons, both of which form H_2^+, which rapidly combines with free electrons to undergo dissociative recombination. Advection moves the dissociation front to lower column densities than in the static case, which vastly increases the heating in the partially molecular gas due to photoionization of He^0, H_2, and H^0. This causes a significant fraction of the incident bolometric flux to be reradiated as thermally excited infrared H_2 lines, with the lower excitation pure rotational lines arising in 1000 K gas and higher excitation H_2 lines arising in 2000 K gas, as is required to explain the H_2 spectrum of the Helix cometary knots.

Subject headings: hydrodynamics — molecular processes — planetary nebulae: individual (NGC 7293)

1. INTRODUCTION

The ultraviolet photons from hot stars, such as main-sequence OB stars or the central stars of planetary nebulae (CSPN), will dissociate and ionize the surrounding circumstellar and interstellar gas. In the classical picture (e.g., Hollenbach & Tielens 1997), the extreme ultraviolet (EUV) photons with energies $h\nu > 13.6$ eV photoionize the hydrogen gas, forming an H II region bounded by a relatively sharp ionization front (IF), while the far-ultraviolet (FUV) photons with energies 6 eV $< h\nu <$ 13.6 eV penetrate the IF to form a neutral photodissociation region (PDR) that surrounds the H II region. The dissociation of H_2 in such a PDR is dominated by a two-step radiative process (Stecher & Williams 1967; Abgrall et al. 2000), in which absorption of an FUV photon leaves the H_2 molecule in an electronically excited state, from which it has a certain probability ($\simeq$10%) of decaying to the vibrational continuum of the ground electronic state.

However, as shown by Bertoldi & Draine (1996), a classical extended PDR cannot exist if the FUV flux is sufficiently weak compared with the EUV flux at the IF; rather, the IF and dissociation front (DF) should merge. Bertoldi & Draine considered the case of H II regions around OB stars and found that this regime was most relevant for cases in which the dust optical depth through the ionized gas is low, which corresponds to a low-ionization parameter (the ionization parameter is a dimensionless number equal to the ratio of the number density of ionizing photons to the number density of hydrogen nuclei). To date, no models have been calculated of the structure and emission properties of such fronts, which are also expected to show strong deviations from static chemical and ionization equilibrium.

In this paper, we calculate in detail the internal dynamics and chemistry of merged ionization/dissociation fronts (IF/DFs), concentrating on the particular case of compact photoevaporating molecular knots in evolved planetary nebulae (PNe) such as those seen in the Helix Nebula (Young et al. 1999; Meixner et al. 2005; Hora et al. 2006; O'Dell et al. 2007, hereafter OHF07). The stellar spectrum from the hot central star of a PN is harder than that from an OB star, leading to an EUV luminosity that is much greater than the FUV luminosity. In addition, the ionization parameter of the knots is much lower than is typically seen in H II regions, resulting in very little attenuation of the EUV flux by recombinations in the ionized gas. Both of these factors place the knots firmly in the merged IF/DF regime. The most comprehensive existing theoretical study of PDRs in planetary nebulae is that of Natta & Hollenbach (1998), who present detailed modeling of the time-dependent evolution of an expanding circumstellar shell as the luminosity and spectrum of the CSPN evolves, finding that soft X-rays can be important in exciting the molecular gas at late times. However, OHF07 showed that this is not the case in the Helix, since it is only in the EUV band that the CSPN luminosity is sufficient to excite the knot PDRs. Natta & Hollenbach used an analytic treatment of the H II region, which is assumed to have absorbed all the EUV radiation, and were thus unable to model the case of a merged IF/DF.

2. MODELS

In order to investigate the structure of advective IF/DFs in PNe, we have calculated steady state, plane-parallel slab models using the Cloudy plasma/molecular physics code (Ferland et al. 1998). Details of the computational scheme used to treat the steady state dynamics are given in Henney et al. (2005), and these methods have now been coupled to a hydrogen chemical network (Abel et al. 2005) and combined with the 1893-level model of H_2 described in Shaw et al. (2005).

In this initial study, we restrict ourselves to models with elemental abundances from Henry et al. (1999) that are illuminated by a blackbody source of luminosity 120 $L_\odot$ and an effective temperature of 130,000 K, chosen to match the CSPN

[1] Contains material © British Crown Copyright 2007/MOD, reprinted with permission.

[2] Centro de Radioastronomía y Astrofísica, Universidad Nacional Autónoma de México, Morelia, México.

[3] AWE, Aldermaston, RG7 4PR, UK.

[4] Department of Physics and Astronomy, University of Kentucky, Lexington, KY 40506.

[5] Department of Physics and Astronomy, Vanderbilt University, Box 1807-B, Nashville, TN 37235.

TABLE 1
MODEL INPUT PARAMETERS

Model	D (pc)	u_0 (km s^{-1})	n_0 (cm^{-3})	F_0 (cm^{-2} s^{-1})	λ_{ad}
A10	0.137	10	3162	3.36×10^9	0.94
A06	0.137	6	3162	3.36×10^9	0.56
A03	0.137	3	3162	3.36×10^9	0.28
A01	0.137	1	3162	3.36×10^9	0.09
A00	0.137	0	3162	3.36×10^9	0.00
AA10	0.137	10	1000	3.36×10^9	0.30
B10	0.244	10	1000	1.06×10^9	0.94
B06	0.244	6	1000	1.06×10^9	0.57
B00	0.244	0	1000	1.06×10^9	0.00
C10	0.433	10	316	3.36×10^8	0.94
C06	0.433	6	316	3.36×10^8	0.56
C00	0.433	0	316	3.36×10^8	0.00

NOTE.—Stellar parameters: $L = 120\ L_\odot$, $T_{\rm eff} = 130{,}000$ K, $Q_H = 7.57 \times 10^{45}$ s^{-1}, $Q_{\rm FUV} = 1.33 \times 10^{45}$ s^{-1}.

of the Helix Nebula (Bohlin et al. 1982; adjusted for the trigonometric parallax of 217 pc [Harris et al. 2007]). We have also calculated some models using a Rauch (2003) stellar atmosphere with the same luminosity and effective temperature.

We vary three different model parameters so as to span the range of physical and illumination conditions that are seen in PN knots: distance from the CSPN, D; hydrogen nuclei density at the illuminated face, n_0; and gas velocity at the illuminated face, u_0. Table 1 summarizes the input parameters of our models.[6]

The magnitude of advective effects in the models is, to first order, dependent only on the dimensionless combination: $\lambda_{ad} = n_0 u_0 4\pi D^2/Q_H$, where Q_H is the ionizing photon luminosity of the source. This advection parameter (Henney et al. 2005) is the ratio of particle flux to photon flux, which increases with u_0 and decreases with ionization parameter. The appropriate value of the downstream flow velocity u_0 depends sensitively on the boundary conditions at the illuminated face and on the global geometry of the flow. In the case of a photoevaporating knot with negligible confining pressure on the ionized side, u_0 will be of order the ionized sound speed ($\simeq$10 km s^{-1}), and this is the case we concentrate on in this paper. In the case of a more shell-like configuration of the molecular gas, u_0 would tend to be lower.

3. PREDICTED MODEL STRUCTURE

Figure 1 shows the results from a typical advective model, B06, while Figure 2 shows results from a static model, B00, with exactly the same incident flux and density as B06. For ease of discussion, we divide the model into three broad zones: zone I is closest to the ionizing source and is largely ionized, with a very low molecular fraction; zone II is the dissociation front, in which the hydrogen is half-neutral and half-molecular (for the advective models, this zone is subdivided into IIa and IIb); and zone III is farthest from the ionizing source, where hydrogen is fully molecular. Table 2 shows typical physical conditions in each zone for the advective models.

[6] Note that all flow velocities, u, are in the frame of reference of the IF/DF, but since we find that u becomes very small at great depths, this is also approximately the rest frame of the molecular gas.

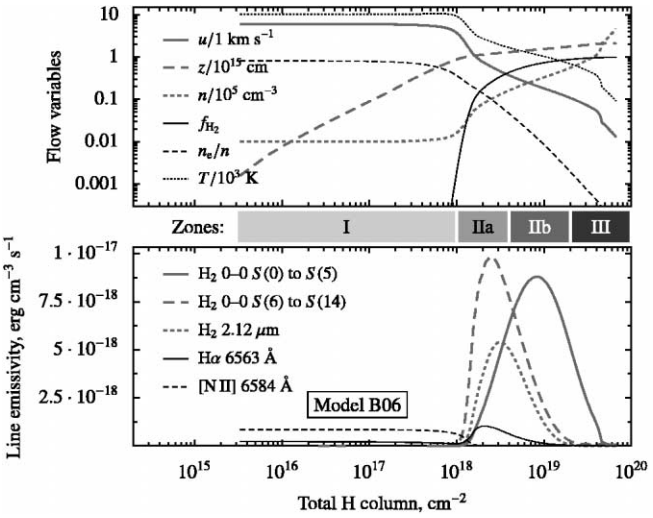

FIG. 1.—Structure of a representative advective model (B06; see Table 1) as a function of column density of hydrogen nuclei. *Top*: Various flow variables on a logarithmic scale: flow velocity u, depth into cloud z, total number density of hydrogen nuclei n, hydrogen molecular fraction f_{H_2}, electron fraction n_e/n, and gas temperature T. *Bottom*: Emissivity of important coolant lines.

The differences between the advective and static models are stark: in the advective model, the DF occurs at the very low column density of 10^{18} cm^{-2} from the illuminated face and strongly overlaps with the ionization front, whereas in the static model the DF occurs much deeper, at 2×10^{19} cm^{-2}, in a region where the ionization fraction is <0.01. Zone II is much warmer in the advective model (2000 K in zone IIa, 1000 K in zone IIb) than in the static model (500 K) and, as a result, H_2 line emission is more than an order of magnitude brighter.

The rates of formation and destruction of H_2 for model B06 are shown in Figure 3, where it can be seen that the destruction rate (*bottom panel*) has a narrow peak at the leading edge of zone IIa, due to collisional processes with protons and electrons, together with a broader peak covering zones IIa and IIb, due to photoionization by hard EUV photons. The principal reaction channel for the H_2^+ ions formed by these processes is dissociative recombination with free electrons (e.g., McCandliss et al. 2007), with only ~10% reacting with H^0 to re-form H_2. Other H_2 formation mechanisms have even smaller rates (*top panel*), with the result that, once they have been destroyed, most H_2 molecules never re-form during the $\simeq$300 yr that they remain in the DF.

The heating and cooling rates for model B06 are shown in Figure 4. In zone I, as is typical for low-excitation H II regions, the heating is dominated by H^0 photoelectric heating, while the cooling is due to H lines and optical metal lines such as [N II] λ6584. In zone IIa, H^0 photoelectric heating still dominates the heating, whereas in zone IIb, photoelectric heating of He^0 and H_2 increasingly take over. In all of zone II the cooling is overwhelmingly dominated by H_2 line emission. In zone III, the heating rate is much lower than in the other zones and is due

TABLE 2
PHYSICAL CONDITIONS IN DIFFERENT ZONES OF A TYPICAL ADVECTIVE IF/DF STRUCTURE

Zone	Column (cm^{-2})	T (K)	u (km s^{-1})	n_e/n	f_{H_2}	n/n_0	Heat	Cool
I	$<10^{18}$	10^4	5	0.6	10^{-6}	1	H^0 p.e.	Metal, H^0 lines
IIa	1×10^{18}–4×10^{18}	2000	0.5	0.1	0.3	10	H^0, He^0, H_2 p.e.	H_2 lines
IIb	4×10^{18}–2×10^{19}	1000	0.2	0.03	0.6	20	He^0, H_2 p.e.	H_2 lines
III	$>2 \times 10^{19}$	200	0.03	3×10^{-4}	0.9	100	H_2 lines	FIR metal lines

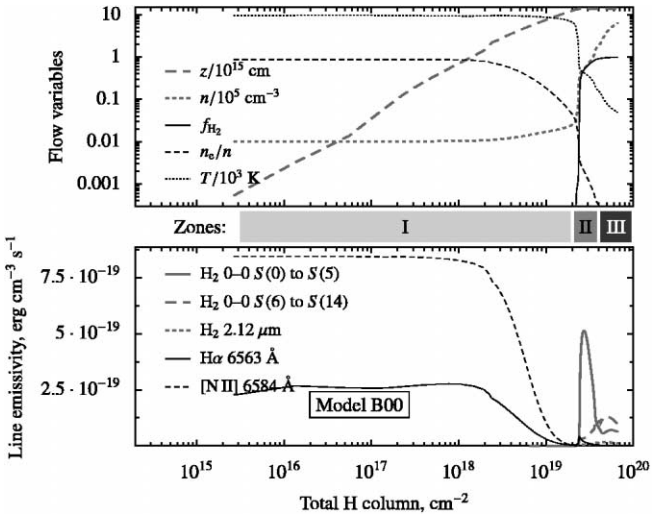

FIG. 2.—Same as Fig. 1, but for an equivalent static model (B00).

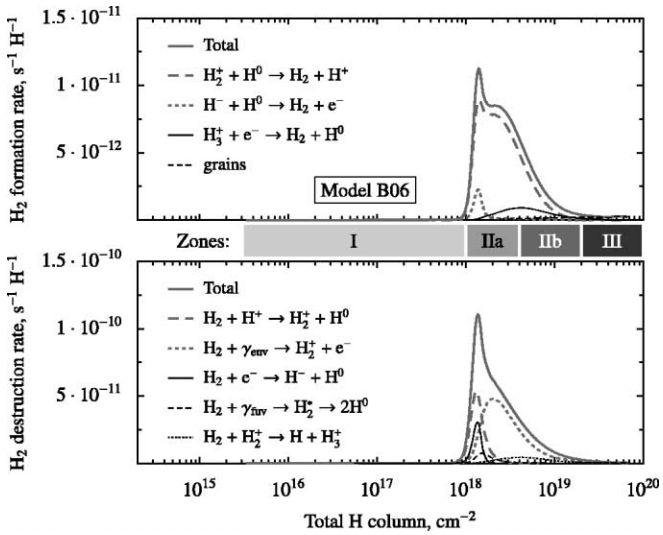

FIG. 3.—Destruction and formation rates of H_2, in units of molecules per hydrogen nucleus per second, for the advective model shown in Fig. 1. *Top*: Formation rates. *Bottom*: Destruction rates. Note the different scales of the *y*-axes.

principally to the absorption of H_2 lines emitted in zone II, while the cooling in zone III is dominated by collisionally excited far-infrared metal lines. Figure 4 (*bottom*) shows the difference between the heating and cooling rates, which is equal to the net rate of energy transfer from the radiation field to the gas. This can be seen to have a sharp peak at the boundary between zones I and IIa, where it represents a significant fraction of the total heating. Outside this narrow heating front, the gas is everywhere in approximate thermal equilibrium. The fraction of the bolometric stellar luminosity that is converted into thermal and kinetic energy of the gas can be shown to be $\simeq \lambda_{ad} T_0/T_{rad}$, where T_0 ($\simeq 10^4$ K) is the zone I gas temperature and T_{rad} ($\simeq T_{eff}$) is the color temperature of the incident radiation. For the model shown, this fraction is 7%, in good agreement with the analytic estimate.

Other advective models show extremely similar structures. The shift in column density of the DF with respect to the static models is roughly proportional to λ_{ad}, but even models with $\lambda_{ad} = 0.09$ have gas temperatures similar to model B06 in zones IIa and IIb. Models using a Rauch atmosphere instead of a blackbody also produced extremely similar results, despite this spectrum having a 20 times smaller flux at soft X-ray wavelengths (>54.4 eV).

A plane geometry is a poor approximation in zone I for the case of photoevaporating knots, in which the ionized flow is expected to be transonic and divergent (O'Dell et al. 2005). However, the small observed spatial offset between the H_2, Hα, and [N II] emission (OHF07) indicates that the flow in zones II and III is approximately plane parallel. The flow timescale through a column density, N, is equal to $N/n_0 u_0 \simeq 32\lambda_{ad}(N/10^{18}\ \mathrm{cm}^{-2})$ yr, which is much less than the PN evolutionary timescale for the H_2-emitting portions of the flow, justifying our steady state assumption. However, nonsteady effects may be important in zone III, as may the formation of CO and magnetic fields, neither of which is included in the present models.

4. PREDICTED H_2 SPECTRUM

Figure 5 shows the radiative efficiency of the models in converting the stellar luminosity into H_2 emission lines: $\eta = L_{lines}/L_*$. The value of η_{tot}, corresponding to the sum of all H_2 lines, is <0.01 for the static models and rises rapidly with λ_{ad} for the advective models, approximately as $\eta_{tot} = 1.1\lambda_{ad}/(1 + \lambda_{ad}^{0.9})$ (Fig. 5, *dashed curve*). The dotted line in the figure indicates the maximum fluorescent efficiency, assuming that all FUV radiation is converted into H_2 lines.

Figure 6 shows predictions of the full H_2 line spectrum for transitions with upper-level excitation temperatures <17,500 K, which includes most near-infrared and mid-infrared lines. Three representative models are shown (Table 1): a static model, C00, and two advective models, C06 and A06, with, respectively, a low and a high incident flux. The line intensities are shown in the standard way as effective column densities, which would be proportional to $\exp(-E_2/kT)$ in the case of a Boltzmann distribution at a single temperature, T, giving a straight line on the semilog plot.

All static models show a typical fluorescent spectrum with strong deviations of the level populations from a Boltzmann distribution, whereas advective models show a much smaller dispersion in the effective columns of levels with similar excitation energies, indicating that the excitation is largely thermal.

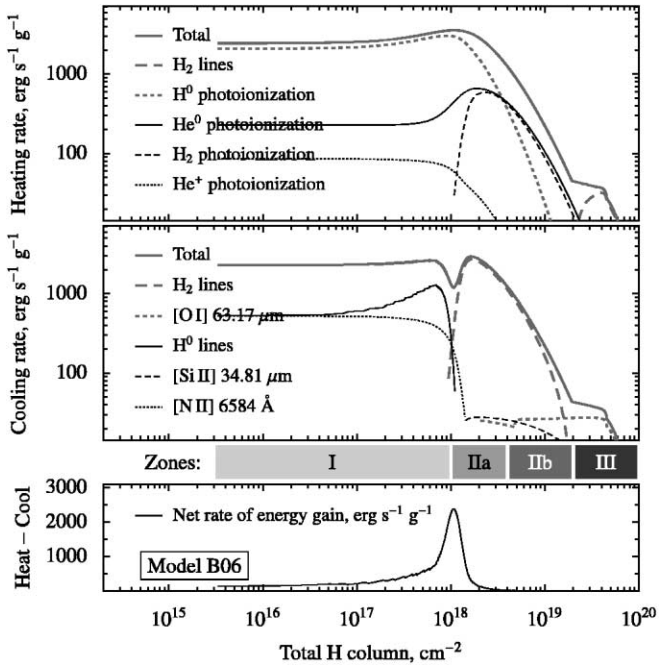

FIG. 4.—Thermal balance of the advective model shown in Fig. 1. *Top*: Principal contributions to the atomic/molecular heating rate per unit mass, shown on a logarithmic scale. *Middle*: Same as top panel, but for cooling rate. *Bottom*: Difference between heating and cooling rates, shown on a linear scale.

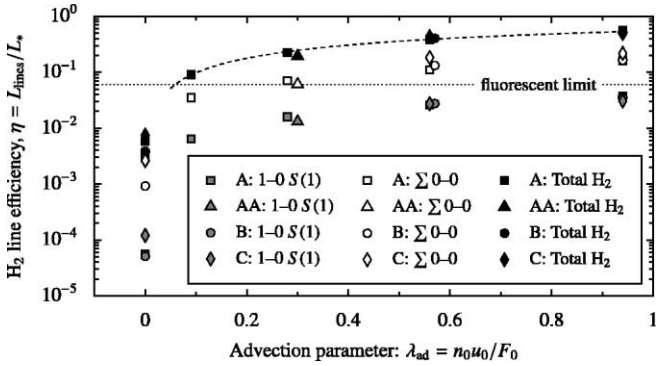

FIG. 5.—Fraction of the stellar bolometric luminosity that is radiated in H_2 lines, assuming 100% covering fraction of molecular gas. Black symbols show the total H_2 line luminosity, white symbols show the sum of the pure rotational 0–0 mid-infrared lines from $S(0)$ to $S(28)$, and gray symbols show the near-infrared 1–0 $S(1)$ line at 2.121 μm. Different symbol shapes are for different sequences of models, as shown in the key. The dashed curve shows an approximate analytic fit (see text).

The slope of the excitation diagram is steeper for lower excitation energies, which is demonstrated in Figure 1: the emissivity of the lower pure rotational lines (excitation temperatures <5000 K) peaks in zone IIb, where the gas temperature is $\simeq$1000 K, whereas higher excitation lines have their peak emissivity in zone IIa, where the gas temperature is $\simeq$2000 K.

5. DISCUSSION

Observations of the molecular hydrogen spectrum of the knots in the Helix Nebula (Cox et al. 1998; Hora et al. 2006; OHF07) are indicated as error bars in Figure 6. It can be seen that the two advective models are in broad agreement with the observations, whereas the static model is not. Model C06 best matches the distance of the spectroscopically observed knots from the ionizing star and indeed shows a better agreement than model A06, which corresponds to the closer-in knots. The observed nebular flux in the 1–0 $S(1)$ line and in the sum of the 0–0 $S(1)$ to $S(7)$ lines is $\simeq$1% and $\simeq$4%, respectively, of the bolometric stellar flux (OHF07). From Figure 5, this can be satisfied by our models with $\lambda_{ad} > 0.3/f$, where f is the area-covering fraction of knots. A strong prediction of our model is that higher excitation lines from the $v \geq 1$ levels should show

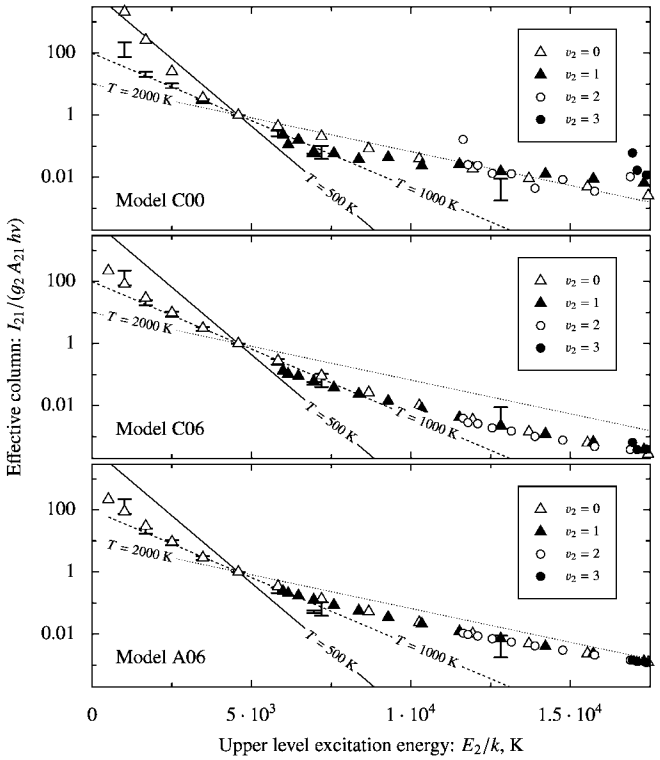

FIG. 6.—Excitation diagrams of H_2 emission lines for three Cloudy models. *Top*, model C00; *middle*, model C06; *bottom*, model A06. Symbols show the predicted effective columns from the Cloudy models, determined from the emergent line intensities, as a function of the excitation temperature of the upper level. Different symbol types indicate the vibrational quantum number of the upper level, v_2, as shown in the key. The effective columns are normalized with respect to the value for the $v_2 = 0$, $J_2 = 7$ level, which gives rise to the 0–0 $S(5)$ line at 6.907 μm. Thin lines show the slope of Boltzmann distributions for 500 K (*solid*), 1000 K (*dashed*), and 2000 K (*dotted*). Error bars show the range of measured values for the Helix knots (see text).

a higher population temperature of $\simeq$2000 K. A recent study of an inner knot (Matsuura et al. 2007) finds a population temperature of about 1800 K for these levels, in agreement with the prediction of our relevant model (A06).

Rovibrationally warm H_2 has been detected in other PNe (e.g., Likkel et al. 2006; McCandliss et al. 2007) and has frequently been interpreted as evidence for shocks (Zuckerman & Gatley 1988). However, EUV-dominated advective PDRs may be a promising alternative in these cases too.

We thank the following institutions and programs for financial support: UNAM, Mexico (PAPIIT IN112006 and IN110108); STScI (GO 10628 and AR 10653); NSF (AST 0607028); NASA (NNG 05-GD81G); and *Spitzer* Science Center (20343).

REFERENCES

Abel, N. P., Ferland, G. J., Shaw, G., & van Hoof, P. A. M. 2005, ApJS, 161, 65
Abgrall, H., Roueff, E., & Drira, I. 2000, A&AS, 141, 297
Bertoldi, F., & Draine, B. T. 1996, ApJ, 458, 222
Bohlin, R. C., Harrington, J. P., & Stecher, T. P. 1982, ApJ, 252, 635
Cox, P., et al. 1998, ApJ, 495, L23
Ferland, G. J., Korista, K. T., Verner, D. A., Ferguson, J. W., Kingdon, J. B., & Verner, E. M. 1998, PASP, 110, 761
Harris, H. C., et al. 2007, AJ, 133, 631
Henney, W. J., Arthur, S. J., Williams, R. J. R., & Ferland, G. J. 2005, ApJ, 621, 328
Henry, R. B. C., Kwitter, K. B., & Dufour, R. J. 1999, ApJ, 517, 782
Hollenbach, D. J., & Tielens, A. G. G. M. 1997, ARA&A, 35, 179
Hora, J. L., Latter, W. B., Smith, H. A., & Marengo, M. 2006, ApJ, 652, 426
Likkel, L., Dinerstein, H. L., Lester, D. F., Kindt, A., & Bartig, K. 2006, AJ, 131, 1515
Matsuura, M., et al. 2007, MNRAS, in press (arXiv: 0709.3065v1)
McCandliss, S. R., et al. 2007, ApJ, 659, 1291
Meixner, M., McCullough, P., Hartman, J., Son, M., & Speck, A. 2005, AJ, 130, 1784
Natta, A., & Hollenbach, D. 1998, A&A, 337, 517
O'Dell, C. R., Henney, W. J., & Ferland, G. J. 2005, AJ, 130, 172
———. 2007, AJ, 133, 2343 (ODH07)
Rauch, T. 2003, A&A, 403, 709
Shaw, G., Ferland, G. J., Abel, N. P., Stancil, P. C., & van Hoof, P. A. M. 2005, ApJ, 624, 794
Stecher, T. P., & Williams, D. A. 1967, ApJ, 149, L29
Young, K., Cox, P., Huggins, P. J., Forveille, T., & Bachiller, R. 1999, ApJ, 522, 387
Zuckerman, B., & Gatley, I. 1988, ApJ, 324, 501